Novel QRS Detection Based on the Adaptive Improved Permutation Entropy

SUBMISSION DATE / POSTED DATE

19-05-2022 / 24-05-2022

CITATION

Mansourian, Nastaran; Sarafan, Sadaf; Ghirmai, Tadesse; Cao, Hung; Torkamani Azar, Farah (2022): Novel QRS Detection Based on the Adaptive Improved Permutation Entropy. TechRxiv. Preprint. https://doi.org/10.36227/techrxiv.19795084.v1

DOI

10.36227/techrxiv.19795084.v1

Novel QRS Detection Based on the Adaptive Improved Permutation Entropy

Nastaran Mansourian, Sadaf Sarafan, *Graduate Student Memeber, IEEE* , Farah Torkamani-Azar*, *Memeber, IEEE*, Tadesse Ghirmai, *Senior Memeber, IEEE* and Hung Cao*,*Senior Memeber, IEEE*

***Abstract*— Detection of the QRS complex is the most important step in analyzing ECG signals for heart monitoring and diagnosis. There have been several QRS-peak detection methods reported in the literature. Most of these methods have low performance under noisy conditions. In this paper, we propose a novel QRS detection algorithm based on a new Permutation Entropy (PE) method that we developed and referred to as the Adaptive Improved Permutation Entropy (AIPE) method. The parameters of the AIPE method are determined based on the specific signal properties. Implementing the AIPE method leads to prominently preserving the QRS complex and eliminating noises of the ECG signal without smoothing the ECG signal. Our simulations show that the proposed QRS detection algorithm is effective and robust under noisy conditions. The algorithm is validated on the MIT-BIH Noise Stress Test Database for various SNR values. In addition, we examined the algorithm's performance under motion noise conditions, mimicking a practical scenario. We used the metrics of sensitivity, positive predictive, and F1 score to evaluate the performance of our algorithm and compare it with several other algorithms explained in the literature. Our investigation shows that the proposed algorithm outperforms other QRS detection algorithms, including the popular Pan-Tompkins algorithm.**

***Index Terms*— Adaptive Improved Permutation Entropy, ECG Analysis, Permutation Entropy, QRS Detection, Signal Processing.**

I. Introduction

ACCORDING to the World Health Organization (WHO), cardiovascular diseases (CVD) are the leading cause of death worldwide, with an estimated 17.5 million deaths per year [1]. More than 80 percent of CVD deaths are due to heart attacks and strokes [1]. Thus, continuous heart rate monitoring is critical for the vulnerable population. Electrocardiogram (ECG) signals provide valuable information such as heart rate (HR) and heart rate variation (HRV) for the diagnosis of CVDs. Furthermore, according to recent research, the COVID-19 pandemic is associated with a rapid reduction in cardiovascular diagnostic procedures across the world [2]. Thus, in unique scenarios such as the current global COVID-19 pandemic, the availability of distanced care and mobile health (m-Health) are critical. As the m-healthcare field develops, mobile ECG devices will become more popular, beckoning novel approaches to assess HR from ECG in practical scenarios in daily life.

ECG signals comprise distinct components: P waves, QRS complexes, and T waves. ECG assessment for diagnosis includes determining heart rate (HR) which is usually achieved by detecting the QRS complex. ECG recordings are commonly contaminated with artifacts such as power-line interference, baseline wander, motion artifacts, among others. In a strong noise setting (low signal to noise ratios - SNR), the detection of QRS complexes could be very challenging [3]. Various techniques have been developed for QRS complex detection, including methods based on the neural networks [4], [5], the wavelet transforms [6], [7], digital filter and filter banks [8], [9] and Hilbert transforms [10], [11]. The neural networks provide remarkable accuracy improvement, however these methods seem to be characterized by mathematical complexity [12]. By using the wavelet transform, good detection ratios can be obtained. Nevertheless, the high required time and memory make it impossible to use this method for real-time applications [13]. Most algorithms based on digital filters are sensitive to the presence of noise [14], [15]. Although Hilbert transforms methods perform greatly, the QRS detection would be challenging during low-amplitude R-wave and ischemic heart conditions [16]. However, all these methods have some drawbacks, such as having high computation complexity, large memory requirement, and particularly low accuracy due to low SNR and motion noise sensitivity [17].

Permutation Entropy (PE) is a quantitative tool that measures system complexity. Although its initial classical method is deprecated, but the other ordinary permutation entropy approaches are now being used [18]. In this paper, we propose and develop a novel permutation entropy-based algorithm for QRS complex detection from ECG signals. The proposed algorithm is based on a new method known as the Adaptive Improved Permutation Entropy (AIPE). We have developed this novel method by extending the Improved Permutation Entropy (IPE) by addressing its shortcomings to detect signals of sharp slope such as the QRS complex [19]. We have performed investigations to demonstrate that the proposed

*Corresponding authors: Farah Torkamani-Azar, Hung Cao.

Nastaran Mansourian is with the Faculty of Electrical Engineering, University of Shahid Beheshti, Tehran, Iran (e-mail: se.mansourian@mail.sbu.ac.ir).

Sadaf Sarafan is with the Department of Electrical Engineering and Computer Science, University of California, Irvine, CA 92697, USA (e-mail: ssarafan@uci.edu).

Farah Torkamani-Azar is with the Faculty of Electrical Engineering, University of Shahid Beheshti, Tehran, Iran (e-mail: f-torkamani@sbu.ac.ir).

Tadesse Ghirmai is with the Division of Engineering and Mathematics, University of Washington, Bothell Campus, Bothell, WA 98011, USA (e-mail: tadg@uw.edu).

Hung Cao is with the Department of Electrical Engineering and Computer Science, University of California, Irvine, CA 92697, USA and Department of Biomedical Engineering, University of California, Irvine, CA 92697, USA (e-mail: hungcao@uci.edu).

algorithm outperforms the Pan-Tompkins algorithm which is the most popular QRS detection method, particularly with low-SNR signals. In the following, PE theorem is defined in section (II), firstly. Then, AIPE as a modified version of PE is presented in section (III), and in residual sections, the implementation and experiments are explained.

II. An Overview of Permutation Entropy

When analyzing a system, the determination of the complexity of its time series signal plays an important role in understanding its characteristics [20]. Entropy is among the most popular complexity measurement methods for signal analysis. It reveals the irregularities and uncertainties of time series signals [21]. To date, various entropy measurement approaches have been proposed, including permutation entropy (PE) [22], sample entropy [23], approximate entropy [23] and entropy of symbolic dynamics (SymDyn) [24]. Compared to all the other entropy algorithms, PE is the most popular method because it is conceptually simple and computationally fast. In addition, PE can be applied to all types of signals, including deterministic, stationary and non-stationary stochastic, and chaotic signals [25].

First introduced in 2002 by Bandt and Pompe, PE combines symbolic patterns and concepts of entropy to create a new method for complexity measurement [22]. To explain the PE algorithm, let us consider a time series signal denoted as

$$\mathbf{x} = \{x(i)\}_{i=1}^{N} \tag{1}$$

where N is the length of the time series. The first step in calculating the permutation pattern is selecting the embedding dimension m and the time delay τ for the time series. The $m \times j$ reconstruction matrix for the signal $\mathbf{x}$ is then given by

$$\mathbf{X} = \begin{bmatrix} x(1) & \cdots & x(j) \\ x(1+\tau) & \cdots & x(j+\tau) \\ \vdots & \ddots & \vdots \\ x(1+(m-1)\tau) & \cdots & x(j+(m-1)\tau) \end{bmatrix} \tag{2}$$

where $j = N - \tau(m-1)$ denotes the total number of columns of the reconstruction matrix. We refer to the columns of the reconstruction matrix as reconstruction vectors, and the k^{th} reconstruction vector is denoted by

$$\mathbf{X}_k = [x(k), x(k+\tau), ..., x(k+\tau(m-1))]^\top \tag{3}$$

Without loss of generality, we assume $\tau = 1$. The first step in defining the k^{th} permutation pattern is to arrange the reconstruction vector $\mathbf{X}_k$ in descending order as

$$x(k+(l_1-1)) \leq x(k+(l_2-1)) \leq ... \leq x(k+(l_m-1)) \tag{4}$$

where l_i is an index that denotes the location in the column $\mathbf{X}_k$ of the i^{th} element of the vector arranged in descending order. For example, suppose $\mathbf{z} = \{5, 1, 8\}^\top$ is one of the columns of (2). After arranging $\mathbf{z}$ in a descending order, the first element of the ordered vector is the second element of $\mathbf{z}$, and the second element of the ordered vector is the first element of $\mathbf{z}$ and the third element of the ordered vector is the third element of $\mathbf{z}$. Thus, we write the indices as $l_1 = 2, l_2 = 1$ and $l_3 = 3$. It is important to note that if two elements of the reconstruction vector are equal, $x(k+(l_{q1}-1)) = x(k+(l_{q2}-1))$, we consider $x(k+(l_{q1}-1)) < x(k+(l_{q2}-1))$ when $l_{q1} < l_{q2}$. For each reconstruction vector $\mathbf{X}_k$, we assign a vector of permutation pattern $\boldsymbol{\pi}^{(k)}$ whose elements are the index of reconstruction vector l_i for $i = 1, 2, ..., m$ as follows,

$$\boldsymbol{\pi}^{(k)} = [l_1, l_2, ..., l_m]^\top \tag{5}$$

Based on permutation principle, there are $m!$ different possible permutation pattern vectors attributed to $\mathbf{X}_k$. The second step in the PE calculation is the estimation of entropy. We denote the probability of the permutation pattern vector of $\boldsymbol{\pi}_i$ as p_i, where $1 \leq i \leq m!$, computed from the relative frequency of occurrence of the pattern in the permutation matrix. The entropy is calculated according to Shannon's rule as [26],

$$H_{PE}(m) = \frac{-\sum_{i=1}^{h}[p_i \times ln(p_i)]}{ln(m!)} \tag{6}$$

where $h \leq m!$ and $ln(m!)$ represents the maximum value of $H_{PE}(m)$, which is in the range of $0 \leq H_{PE}(m) \leq 1$. Despite the significant success of Bandt's PE method in various fields, it has serious limitations to be applicable in a wide range of applications. Some of these drawbacks are the following:

1) The first definition of PE, which Bandt and Pompe introduced, is based on single time scale signals. Hence, it is ineffective for complex systems with multiple time scale signals [27].
2) The original PE algorithm was proposed for continuous-time signals in which the incidence of equal values is rare and, hence, can be ignored. But, in most practical applications, we deal with digitized signals. Depending on the amplitude resolution, such signals are likely to have more similar or equal values, and if not properly accounted for, can introduce bias in PE estimation [28], [29]. *E.g.*, according to the original PE method, the two vectors $\mathbf{z}_1 = \{1, 2, 3, 4\}^\top$ and $\mathbf{z}_2 = \{1, 2, 2, 2\}^\top$, are both transformed to the same pattern $\boldsymbol{\pi}_1 = \{0, 1, 2, 3\}^\top$, although $\mathbf{z}_1$ is quite ascending compared to $\mathbf{z}_2$.
3) Amplitude and slope information of signals were ignored in the initial definition of PE [30]–[33]. For example, the same ordinal pattern $\boldsymbol{\pi}_1 = \{0, 1, 2\}^\top$ is assigned to all symbols shown in Fig. 1.
4) The PE method is susceptible to noise because it assigns two different ordinal patterns to signals such as $\mathbf{z}_1 = \{1, 1.001, 1.02\}^\top$ and $\mathbf{z}_2 = \{1.001, 1.02, 1\}^\top$. This characteristic of the PE method renders it useless especially for bio-signals that acquired in real-life settings because they possess a variety of noises and interference, including motion artifacts [34], [35].

All these drawbacks limit the use of PE. Consequently, there have been efforts coming up with modified methods that address the limitations of the original PE [36]. For example, to solve the single time scale limitation of the original PE, Zunino *et al.* proposed a scale-dependent scheme by generalizing the computation of the PE to different embedding delays [37]. Similarly, Aziz presented another method, known as multiscale PE (MPE), which estimates the PE in different time scales. This is accomplished by introducing a time-scale factor

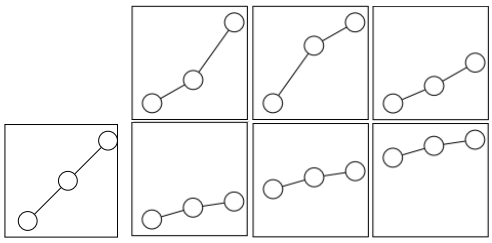

(a) (b)

Fig. 1. $\boldsymbol{\pi_1}$ corresponds to different modes for $\boldsymbol{m = 3}$. (a) $\boldsymbol{\pi_1 = \{0, 1, 2\}}$ pattern. (b) Other possible situations.

and dividing the time series into several coarse-grained time series [38]. The weighted-PE (WPE) [30], proposed in 2013, addressed the original PE limitation of discarding amplitude and slope information of signals by introducing weight to each ordinal pattern. Another method known as the amplitude-aware PE (AAPE) was also proposed in 2013 [32] to address the same limitation.

Depending on amplitude resolution, the way equal values are assigned ordinal patterns is the most serious limitation of the original PE method because it introduces bias in estimating the entropy. To address this issue, Bian *et al.* defined a modified permutation entropy (mPE) [39] which assigns the same symbols to equal values in the pattern vector. Despite its solution to the issue of equal values, mPE has other drawbacks. First, although White Gaussian Noise (WGN) is completely random, mPE does not assign the maximum entropy value to WGN. Moreover, it does not incorporate amplitude information in computing entropy.

III. Method

Before delving into the QRS detection algorithm, in this section, we explain the AIPE method, which is the basis for the algorithm. The AIPE algorithm can be seen as an extension of the Improved Permutation Entropy (IPE) method [19].

A. Improved Permutation Entropy

The determination of the permutation patterns of the IPE algorithm involves quantization of the time series signal values. Consider a quantization function $Q(x)$ as shown in (7),

$$\begin{aligned} Q(x_i) &= l \quad , x_{min} + l\Delta \leq x(i) < x_{min} + (l+1)\Delta \\ \Delta &= (x_{max} - x_{min})/L \end{aligned} \tag{7}$$

where x_{min} and x_{max} represent the minimum and maximum values of the time series $\mathbf{x} = \{x(i)\}_{i=1}^{N}$, respectively. The number of quantization levels is denoted by L, and Δ is the spacing between the quantization levels. The quantization $Q(x)$ function converts each value of the time series $\mathbf{x} = \{x(i)\}_{i=1}^{N}$ into an integer digit l whose value is $0 \leq l \leq L-1$. To determine the permutation patterns, the first step is to digitize the first row of the reconstruction matrix $\mathbf{X}(1,:)$ by $Q(x)$ function and place it in the first row of the permutation matrix $\mathbf{\Pi}(1,:)$. Afterwards other rows of the permutation matrix $\mathbf{\Pi}(n,:)$, where $2 \leq n \leq m$ are obtained from (8), based on the first row of reconstruction matrix, $\mathbf{X}(1,:)$.

$$\begin{aligned} \mathbf{\Pi}(n,k) = \mathbf{\Pi}(1,k) + \left\lfloor \frac{\mathbf{X}(n,k) - \mathbf{X}(1,k)}{\Delta} \right\rfloor \\ 1 \leq k \leq N - \tau(m-1) \qquad , 2 \leq n \leq m, \end{aligned} \tag{8}$$

where $\lfloor \cdot \rfloor$ is the floor operator. Each column of the permutation matrix $\mathbf{\Pi}$ corresponds to one of the possible permutation patterns $\boldsymbol{\pi}_i$, where $1 \leq i \leq L^m$. Once the improved permutation patterns are defined, the entropy is computed using

$$H_{IPE}(m) = \frac{-\sum_{i=1}^{h}[p_i \times ln(p_i)]}{ln(L^m)} \tag{9}$$

where $h \leq L^m$, $ln(L^m)$ shows the maximum value of H_{IPE} and p_i is the probability of pattern $\boldsymbol{\pi}_i$, which is computed from the relative frequency occurrence of $\boldsymbol{\pi}_i$ in $\mathbf{\Pi}$. However, IPE solves the equal values limitation of the original PE method and incorporates amplitude and signal fluctuation information in the computation of entropy, but it has the following shortcomings: (I) Digitization levels of the amplitude, and slope information are not independent of each other; (II) WGN is not assigned the maximum value of IPE, there is a slight deviation as shown in Fig. 2(a). Since white Gaussian noise is a completely random signal, the WGN must get a maximum absolute value according to the entropy definition. (III) Signal fluctuations are not independently taken into account.

B. Adaptive Improved Permutation Entropy

We propose a novel method, AIPE, that like the other PE approaches, its computation has two parts: (I) pattern definition; (II) entropy calculation. AIPE defines the first row of the permutation matrix $\mathbf{\Pi}(1,:)$ in the same way as the IPE, except that a new parameter th_{slope} is added to make the slope information independent of the amplitude information. The parameter th_{slope} is determined from the slope of the signal.

If the absolute difference of the values of two consecutive samples of the vector $\mathbf{X}(:,k)$ is less than th_{slope}, the two samples are assigned equal digital values; otherwise, a digital value of the second sample is determined by adding the integer parts of $(\mathbf{X}(n,k) - \mathbf{X}(n-1,k))/th_{slope}$ to the digital value

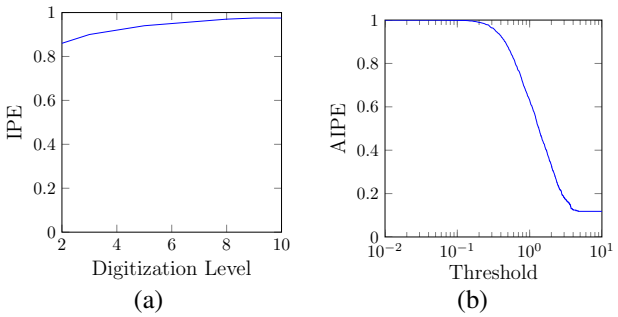

(a) (b)

Fig. 2. (a) Inability of IPE to assign maximum entropy value to WGN. For $\boldsymbol{\tau = 1}$ and $\boldsymbol{m = 4}$. (b) Assigning maximum AIPE value to WGN. For $\boldsymbol{m = 4}$, $\boldsymbol{L = 3}$ and $\boldsymbol{\tau = 1}$.

of the first sample as:

$$\mathbf{\Pi}(n,k) = \mathbf{\Pi}(n-1,k) + sgn(\frac{\mathbf{X}(n,k) - \mathbf{X}(n-1,k)}{th_{slope}}) \times \left\lfloor \frac{|\mathbf{X}(n,k) - \mathbf{X}(n-1,k)|}{th_{slope}} \right\rfloor \quad 1 \le k \le N - \tau(m-1) \quad and \quad 2 \le n \le m. \tag{10}$$

where $sgn(.)$ represents the sign function and $sgn(w)\lfloor |w| \rfloor$ shows the integer part of w.

To illustrate the difference between IPE and AIPE permutation pattern assignments, let us take the vector $\mathbf{X}(:,z_1) = \{1.2, 0, 1.6, 4\}^\top$ as an example, where $m = 4$. Assuming $L = 4$, the permutation pattern assignment by IPE is $\mathbf{\Pi}(:,z_1) = \{1,0,1,3\}^\top$. However, the permutation pattern of AIPE depends on the parameter th_{slope} whose value is based on signal slope with accounting for signal fluctuations. For example using $th_{slope} = 0.5$, the AIPE permutation pattern of the vector $\mathbf{X}(:,z_1)$ is $\mathbf{\Pi}(:,z_1) = \{1,-1,2,6\}^\top$, whereas for $th_{slope} = 2$, the AIPE permutation pattern of $\mathbf{X}(:,z_1)$ becomes $\mathbf{\Pi}(:,z_1) = \{1,1,1,2\}\top$.

It is also worth mentioning that AIPE assigns the maximum entropy value to WGN for appropriately chosen th_{slope} even for small amounts of L. Figure 2(b) shows the plot of the AIPE entropy of WGN versus th_{slope} for $m = 4$, $L = 3$, $\tau = 1$. As seen in the figure, the AIPE entropy is the largest possible value of 1 for a range of the th_{slope} values.

To summarize the discussion of the generation of the AIPE permutation patterns, we recall that a time series signal is first mapped to a reconstruction matrix with j columns referred to as reconstruction vectors. A permutation pattern $\boldsymbol{\pi}^{(k)}$ is determined for each of the reconstruction vector $\mathbf{X_k}$ to make up the permutation matrix $\mathbf{\Pi}$. For a given m and L, the number of possible permutation patterns $\boldsymbol{\pi}_i$ is $1 \le i \le max\{L,d\}^m$ where $d = \lfloor (x_{max} - x_{min})/th_{slope} \rfloor$. After finding the probability for each permutation pattern, p_i, which is determined from the relative frequency of occurrence of the patterns in $\mathbf{\Pi}$, the normalized AIPE entropy is computed as:

$$H_{AIPE}(m) = \frac{-\sum_{i=1}^{h}[p_i \times ln(p_i)]}{ln(max\{d,L\}^m)} \tag{11}$$

where $h \le max\{d,L\}^m$. We note that the maximum value of $H_{AIPE}(m)$ is obtained when $\mathbf{x} = \{x(i)\}_{i=1}^N$ has a uniform distribution.

IV. Implementation

Here, QRS complex detection based on the proposed AIPE method is presented. After applying the AIPE method to an ECG signal, we preserve the QRS complex and eliminate all other parts of the signal, including noise. Then, Q, R, and S waveforms are identified based on amplitude to detect the QRS complex. Before this, it is necessary to pre-process the signal to remove undesired components.

A. ECG Pre-processing

A wide range of noise sources affects a recorded ECG signal, including external electrical interferences (higher frequencies), muscular activity or breathing (lower frequencies) [40]–[42]. The low-frequency noise is more pronounced when the subject is exercising. Baseline wander at lower than $1Hz$ [43] is removed by using a second-order zero-phase low-pass filter with a cut-off frequency of $1Hz$. The output of the low-pass filter is the estimate of the baseline wander, which is subtracted from the ECG signal to obtain the pre-processed ECG signal [44], [45].

B. Applying AIPE to ECG signal

When the AIPE method is applied to the pre-processed ECG signal, it keeps the QRS complex intact while removing all the undesired parts of the signal. The AIPE method exploits the high amplitude and steep slope of the time-domain characteristics of the QRS complex to extract it from the noise without scaling down the R-peak. It is important to note that if instead, a low-pass filter is used to remove the noise of the ECG signal, it is challenging to find a suitable cut-off frequency that does not smooth out and affect the morphology of the ECG wave. Below, we provide details of the multiscale AIPE method that removes the undesired features of an ECG signal.

1) Set AIPE Parameters: The first step in implementing the AIPE method is determining a few important parameters.

(I) We should determine the parameter th_{slope} that represents the threshold of the slope of the QRS complex of the signal. The QRS complex has a high slope, which is a unique feature that helps in its detection as well as the elimination of the other undesired features of the ECG signal. Suppose $\mathbf{x}$ and $\mathbf{x}'$ denote the first two seconds of the pre-processed ECG signal and its derivative,

$$\mathbf{x} = [x(1), x(2), ..., x(2f_s)] \tag{12}$$

The maximum amplitude of vector $\mathbf{x}$ is denoted by

$$max(\mathbf{x}) = x(n). \tag{13}$$

where n shows the position of maximum amplitude of $\mathbf{x}$. Assuming the width of a healthy QRS is $0.1f_s$, we denote the subsequence of the two-second-long pre-processed ECG signal that consists of the QRS complex as (14)

$$\mathbf{x}_{QRS} = [x(n - \lfloor 0.05 \times f_s \rfloor), ...x(n), ..., x(n + \lfloor 0.05 \times f_s \rfloor)] \tag{14}$$

Finally, we use the following closed-form expressions to compute th_{slope}

$$th_{slope} = \sqrt{|\mathbf{x}'_{QRS}|_2^2} \tag{15}$$

where $|.|_2$ represents norm of the signal with order two. (II) The number of quantization levels used to digitize the amplitude of the signal is set to $L = 5$; (III) We select the embedding dimension $m = 3$. Recall that Bandt and Pompe suggested the embedding dimension to be between $3 \le m \le 7$; (IV) We set $\tau = 1$, a value that commonly selected to maintain the signal structure; (V) Since the regular QRS complex duration is 30-100 ms [46], the subsequence length used to calculate the multiscale AIPE is recommended to be equal to half of the width of the QRS complex length. In this study, we select the subsequence length $s = \lfloor 0.05 \times fs \rfloor$.

2) AIPE Implementation: To implement the multiscale AIPE method with the parameters specified in the previous section, we follow the steps outlined below:

1) The pre-processed ECG signal is divided into subsequences of length s, and each consecutive subsequence overlaps by $s-1$ samples resulting in a total of $N-(s-1)$ subsequences. We note that each subsequence with length s generates a single entropy number.
2) Each subsequence determined in the previous step is mapped to a reconstruction matrix $\mathbf{X}$. Since $m=3$ and $\tau=1$, as specified in the last subsection, the dimension of the matrix $\mathbf{X}$ is equal to $3\times(s-2)$.

$$\mathbf{X}^{(k)}=\begin{bmatrix} x(k+1) & \cdots & x(k+s-2) \\ x(k+2) & \cdots & x(k+s-1) \\ x(k+3) & \cdots & x(k+s) \end{bmatrix} \tag{16}$$

   Where $0\leq k\leq N-(s-2)-2$.
3) The first row of matrix $\mathbf{X}^{(k)}$ is mapped to the first row of the permutation matrix $\mathbf{\Pi}^{(k)}$ of the k_{th} subsequence using (7). It should be noted that since a QRS complex with a negative R-peak indicates a reversal of the ECG recording, the $Q(\cdot)$ function is performed on the absolute value of the pre-processed ECG signal. That means the maximum and minimum values of the ECG signal are computed based on the absolute values of the pre-processed ECG signal.
4) The other elements of each column of the matrix $\mathbf{\Pi}^{(k)}$ are computed using (10). These values represent the integer part of the difference between consecutive samples of the ECG signal normalized by the th_{slope} value.
5) Finally, an entropy value is computed for each $\mathbf{\Pi}^{(k)}$ using (11).

Recall that the first row of the permutation matrix $\mathbf{\Pi}$ is obtained by quantizing consecutive samples of the Q of the signal whose length is selected to be small, $s=\lfloor 0.05\times f_s\rfloor$, to consider only small-scale changes. As a result, if the variation in a subsequence is mainly due to noise, since the amplitude does not change much, the elements of the first row of the corresponding $\mathbf{\Pi}$ are generally equal. Furthermore, the other rows of $\mathbf{\Pi}$ of such a subsequence would be equal to the first row because the change in consecutive samples of the signal is almost less than th_{slope}. Consequently, for subsequence varying due to noise, all the columns of its corresponding permutation matrix are equal, and thus, its entropy is equal to zero. However, if a subsequence includes samples from the QRS complex, the first row of the matrix $\mathbf{\Pi}$ takes different values because the QRS amplitudes change rapidly. Moreover, since the slope of the QRS complex is sharp, the other elements of each column of $\mathbf{\Pi}$ are not equal to the first element of the corresponding column, and also the values of each column of $\mathbf{\Pi}$ are different. Therefore, unlike the noise subsequence, the entropy of a QRS subsequence is non-zero.

After implementing the above steps for each sub-sequence s, the multiscale entropy length, referred to as the AIPE sequence, equals $N-(s-1)$, which is $s-1$ samples shorter than the length of the pre-processed ECG signal. Zero padding is applied at the beginning and end of the AIPE sequence so that its length equals the ECG signal.

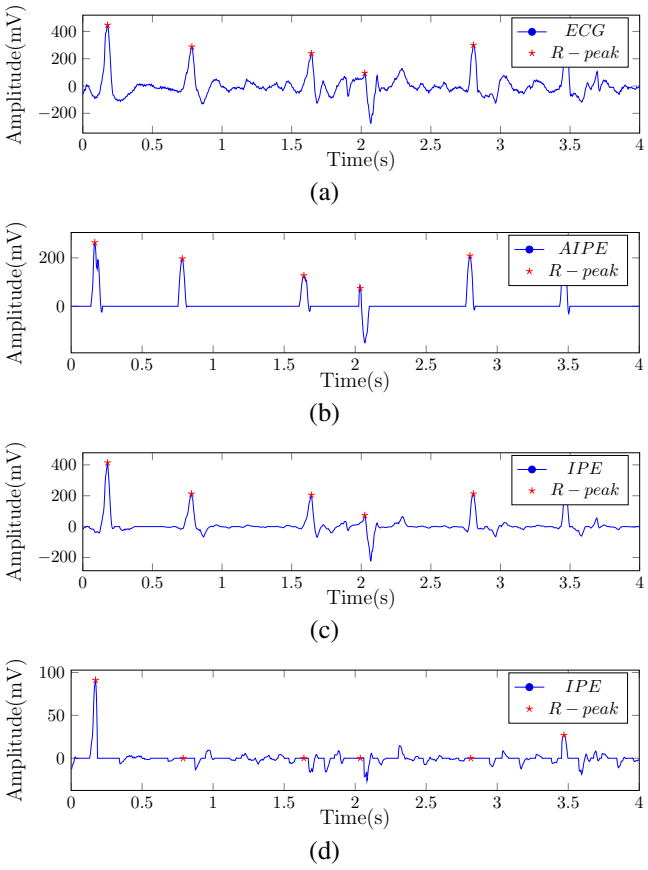

Fig. 3. The importance of defining the $\boldsymbol{th_{slope}}$ independently for detecting QRS complex. (a) Tape 203 of MITDB modified by motion noise. (b) AIPE signal of tape 203 of MITDB with the above-mentioned parameters. (c) IPE processed signal of tape 203 of MITDB with $\boldsymbol{L=5}$. (d) IPE processed signal of tape 203 of MITDB with $\boldsymbol{L=\lfloor th_{slope}\rfloor}$.

3) Detection: Once the AIPE sequence is obtained, it is multiplied by the pre-processed ECG signal to generate the AIPE processed signal, which preserves only the QRS complexes and completely suppresses the rest of the signal by setting it to zero, even when the signal-to-noise ratio (SNR) of the recorded ECG is low. Fig. 3(a) shows the pre-processed ECG signal obtained from tape 203 of the MIT-BIH Arrhythmia database (MITDB) modified with motion noise artifact, and Fig. 3(b) depicts the result after the signal of Fig. 3(a) is AIPE processed by setting $L=5$ and $th_{slope}=\sqrt{|\mathbf{x}'_{QRS}|_2^2}$ which suppresses noise and other parts of ECG signal except QRS complex. Furthermore, Fig. 3(c) and Fig. 3(d) display the outputs of IPE processing of the signal of Fig. 3(a) using two different values of L, $L=5$ and $L=\lfloor th_{slope}\rfloor$, respectively. Both figures highlight the importance of defining a slope parameter, such as th_{slope} defined in AIPE method, independent of L. As in the case of the IPE method, where no slope parameter is specified, if the value of L is set high, Δ will be small, and all parts of the ECG signal whose slope is greater than Δ would appear as QRS complexes. On the other hand, if Δ is set high, L will be small, and the first row of the matrix $\mathbf{\Pi}$ for noisy subsequence would not remain fixed, and the noise would not be suppressed in the processing.

C. Decision

Once the AIPE processed signal is obtained, the next step is to identify the R-peaks of the signal. A robust algorithm for determining the R-peaks is essential, especially for low SNR signals where noise with high amplitude and steep slope can be incorrectly detected as R-peak. We use a decision method similar to the Pan-Tompkins algorithm to choose the R-peaks. The identification of the R-peaks involves initial setting and periodic adjusting of the amplitude and R-peak to R-peak (R-R) interval thresholds.

1) Adjusting Amplitude Thresholds: Two amplitude thresholds are set to ensure the R-peaks are selected correctly. The highest amplitude threshold, denoted as th_{Rpeak}, is first used, and a peak whose amplitude greater than th_{Rpeak} is considered as R-peak to finding the corresponding QRS complex. However, if no QRS is identified in a specified time interval, 1.66 times the average R-peak to R-peak interval, the peaks whose amplitude greater than the lowest threshold, denoted th_{noise}, will be examined by a search-back technique. It should be noted that any peak whose amplitude is less than th_{noise} is definitely noise.

Initially, the threshold values are determined as follows. Suppose $\mathbf{y}$ denotes the first two-second subsequence of the AIPE processed signal, and n denotes the position where $\mathbf{y}$ gets its maximum value, the values of th_{Rpeak} and th_{noise} are calculated as shown by equations (17) and (18), respectively,

$$th_{Rpeak} = \frac{y(n)}{3} \tag{17}$$

$$th_{noise} = \frac{\sum_{i=1}^{2\times f_s} y(i)}{4 \times f_s} \tag{18}$$

The amplitude thresholds are adjusted continuously based on the past R-peaks and noise peaks. Suppose $PEAK$ denotes the amplitude of the R-peaks, and $NOISE$ denotes the amplitude of the noise peaks. After detecting at least three R-peaks and noise peaks, the thresholds are updated as follows

$$th_{Rpeak} = 0.875 \times th_{Rpeak} + 0.125 \times \frac{PEAK_{q-2} + PEAK_{q-1} + PEAK_q}{3} \tag{19}$$

$$th_{noise} = 0.875 \times th_{noise} + 0.125 \times \frac{NOISE_{l-2} + NOISE_{l-1} + NOISE_l}{3} \tag{20}$$

where q and l are the indices of the R-peak and noise peaks detected.

2) Adjusting the average R-R interval: Like the Pan-Tompkins algorithm [8], the average R-R interval is estimated by computing the average of the most recent eight detected R-R intervals,

$$RR_{ave} = 0.125 \times (RR_{q-7} + RR_{q-6} + ... + RR_q). \tag{21}$$

Estimating the average R-R intervals helps define the interval over which to search the R-peaks. If no peak greater than th_{Rpeak} threshold is detected in the interval of $1.66 \times RR_{ave}$, we use the lowest threshold th_{noise} to search R-peak whose amplitude is between th_{Rpeak} and th_{noise}. In this case, if the detected peak is larger than the average of the three most recent determined peaks, it is considered the R-peak. It should be noted that since the amplitude of the AIPE processed signal is a function of the amplitude and slope of the original ECG signal, it is likely that the selected R-peak is a T-wave. Therefore, if the R-R interval between two consecutive peaks is less than 360 ms, it should be examined by its amplitude. If the selected R-peak amplitude is less than half of the average of the two most recent detected peaks, it is considered noise (Fig. 4). Also, it is worth noting that the minimum R-R interval must be greater than 200 ms.

V. Experiments, Results and Discussion

A. Data for Testing

1) MIT-BIH Noise Stress Test Database: We validated our algorithm using ECG recordings obtained from the MIT-BIH Noise Stress Test Database (NSTDB) [47]. This database includes twelve half-hour ECG recordings and three half-hour noise signals of typical ambulatory ECG recordings, such as baseline wander, muscle artifact, and electrode motion artifact. The NSTDB noisy recordings are created by adding the noise signals to the clean recordings from tape numbers 118 and 119 of MIT-BIH Arrhythmia Database [48]. The first 5 minutes of each record are left clean, but a noise signal is added on two-minute segments of the recordings alternating with two-minute of the clean signal. The sampling frequency and bit resolution of these signals were set to 360 samples per second and 11 bits resolution over a 10-mV amplitude range. The noisy recordings have SNR ranging from -6 to 24 dB.

2) Modified Signals with Motion Artifacts Added: To evaluate our algorithm under motion noise conditions, we added a real motion artifact to the clean ECG signals of the MIT-BIH Arrhythmia database (MITDB) [48]. The real motion artifact was extracted, using the EKF denoising method, from ECG signals recorded during physical activities such as walking [49]. When adding noise to the ECG signal, applying amplitude normalization is essential, and before adding the motion noise, we normalized the ECG signal to -1 V to 1 V.

B. Comparison Criteria

We use the evaluation metrics $Sensitivity$, $Positive\ predictive$ and $F1$ to compare our algorithm with other methods. $Sensitivity$ shows the ability of the algorithm to detect QRS complexes, and it is given by

$$Se = \frac{TP}{TP + FN} \tag{22}$$

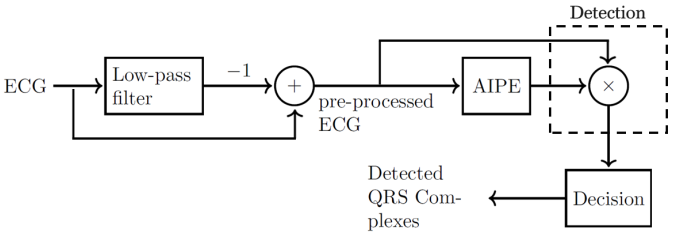

Fig. 4. QRS detection steps using AIPE algorithm.

where TP denotes True Positive, the number of correctly detected true QRS complexes, and FN denotes False Negative, which is the number of QRS complexes not detected. The $Positive\ predictive$ (+P) is a ratio that shows how many of the detected QRS complexes are actually true QRS complexes, and it is given by

$$+P = \frac{TP}{TP + FP} \tag{23}$$

where FP denotes False Positive which represents the number of detected QRS complexes that are not actually QRS complexes. The $F1$ considers both FP and FN indicators. In other words, it is a harmonic mean of FN and FP. Out of the three metrics, $F1$ is the best metric because its value doesn't change considerably if an indicator improves at the expense of the others. $F1$ is defined by,

$$F1 = \frac{TP}{TP + \frac{1}{2}(FP + FN)}. \tag{24}$$

C. Results

To investigate the performance of the proposed algorithms, we conducted multiple experiments. In the first experiment, we run our algorithm using the recorded signal number 118 from NSTDB with varying SNR from -6 to 24 dB. Also, for comparison, we implemented and run the Pan-Tompkins [8], Chen moving average [50], combined adaptive threshold [51] and EMD [52] algorithms on the same recorded signal. As well as, to compare the effect of IPE and AIPE in QRS detection, we implemented an IPE-based QRS detection algorithm. Fig. 5 depicts the performances $F1$, Se, and $+P$ of the proposed algorithm and the other algorithms after applying a signal of different SNR levels. As seen in Fig. 5(a), the proposed AIPE algorithm achieves the highest $F1$ of all the other methods at all SNR levels. We note that the gain of our algorithm in $F1$ compared to the other methods is significant at low SNR levels. Also, Fig. 5(b) depicts that the proposed method provides higher Se than the other methods. Similarly, the plot of $+P$, Fig. 5(c) shows that our algorithm exhibits better performance overall than the other methods. So, generally, we note that the gain in performance of our algorithm over the other methods is significant and more robust at low SNR levels. Furthermore, we conducted an experiment to evaluate the performance of the proposed algorithm under the motion noise conditions. In our experiment, we used the MIT-BIH Arrhythmia database (MITDB) data by adding it to the real motion artifacts. The resulting signal had SNR levels that ranged from -11.5202 to 8.8693. Table I shows in details the data used in this experiment with our algorithm. Table II shows the performance of the various algorithms under motion noise conditions, also. The results shown in the table are the average $F1$, Se, and $+P$ over a range of the SNR levels. The proposed algorithm with average $F1$ = 95.83%, Se = 96.71%, and $+P$ = 95.02% outperforms all the other algorithm, including the popular the Pan-Tompkin algorithm.

We also tested the algorithms using the clean signals from the MIT-BIH Arrhythmia database (MITDB) with no noise added. Table III shows in details the raw data used in this experiment with our algorithm. In the sequel, Table IV shows the performance result of the various algorithms. The proposed algorithm achieves average $F1$ = 95.83%, Se = 96.71%, and $+P$ = 95.02%. Although not as much as in the case of noisy conditions, the proposed algorithm outperforms the other algorithms when no noise is added.

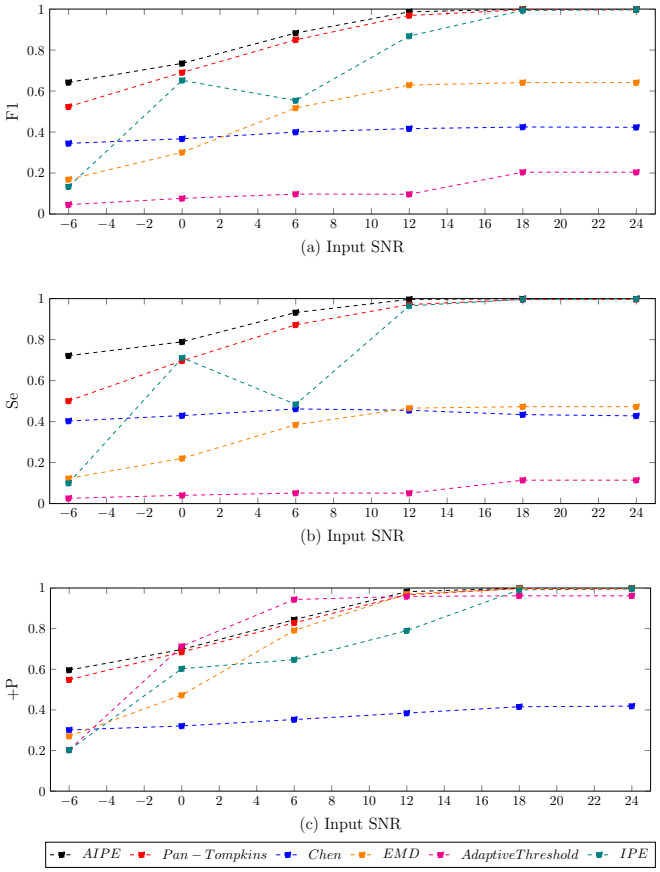

Fig. 5. The AIPE and some other algorithms' comparison applies to data 118 with varying SNRs from -6dB to 24dB. (a) $\boldsymbol{F1}$ metric comparison. (b)$\boldsymbol{Se}$ metric comparison. (c) $\boldsymbol{+P}$ metric Comparison.

VI. Conclusion

In this paper, we have proposed a novel QRS detection algorithm. The algorithm is based on the new permutation entropy method we developed. Through simulations, we have shown that the proposed algorithm is reliable and effective and outperforms several such algorithms, including the popular Pan-Tompkin algorithm. Most importantly, the proposed algorithm is robust under noisy conditions, including motion noise, and shows a significant performance advantage over the other algorithms under such conditions. Furthermore, due to its computational simplicity, the proposed algorithms is suitable for implementation in wearable ECG monitoring devices. In the future, we will implement the algorithm in such a platform.

References

[1] W. H. Organization, "Cardiovascular diseases (cvds) fact sheet," 2017.

TABLE I
RESULTS OF AIPE ALGORITHM FOR QRS DETECTION USING THE MIT-BIH ARRHYTHMIA DATABASE WITH THE MOTION ARTIFACTS ADDED.

Tape	Beats	SNR (dB)	F1	Se	+P
100	2273	3.0549	97.5885%	98.8121%	96.3948%
101	1865	-11.52	93.1408%	96.7846%	89.7614%
102	2187	0.7682	97.4649%	98.5806%	96.3742%
113	1795	2.2744	99.4727%	99.8329%	99.1150%
115	1953	2.1138	98.9095%	99.4391%	98.3855%
118	2275	5.3827	96.2852%	98.4197%	94.2413%
119	1987	7.1671	97.1457%	99.3457%	95.0409%
122	2476	-1.870	98.1622%	99.1525%	97.1915%
123	1518	1.5492	97.5325%	98.9460 %	96.1588%
202	1795	0.4293	92.4814%	95.7905%	89.3933%
208	2956	1.3105	89.9002%	85.9725%	94.2040%
209	3004	6.5638	98.8601%	98.7133%	99.0073%
210	2647	1.0432	84.4075%	83.6957%	85.1315%
212	2748	6.3985	98.3731%	98.5156%	98.2310%
213	3251	7.4797	98.9399%	99.0464%	98.8336%
214	2262	2.9791	95.4387%	96.7415%	94.1706%
217	2208	3.2449	93.7431%	95.7976%	91.7749%
221	2427	8.8693	95.5187%	95.6950%	95.3431%
234	2753	1.8070	97.5566%	98.3339%	96.7914%

TABLE II
RESULTS OF COMPARING THE AIPE ALGORITHM WITH OTHER METHODS FOR QRS DETECTION USING THE MIT-BIH ARRHYTHMIA DATABASE WITH THE MOTION ARTIFACTS ADDED.

Method	F1	Se	+P
AIPE	95.8380%	96.7166%	95.0286%
Pan-Tompkins [8]	94.1557%	95.2281%	93.3704%
Chen *et al.* [50]	51.6787%	55.4814%	55.7182%
EMD [52]	53.9932%	43.3045%	86.3159%
Adaptive Threshold [51]	6.0348%	3.1236%	88.7500%
IPE	91.2486%	92.3277%	91.7645%

TABLE III
RESULTS OF AIPE ALGORITHM FOR QRS DETECTION USING THE MIT-BIH ARRHYTHMIA DATABASE.

Tape	Beats	F1	Se	+P
100	2273	100.0000%	100.0000%	100.0000%
103	2084	100.0000%	100.0000%	100.0000%
112	2539	100.0000%	100.0000%	100.0000%
115	1953	100.0000%	100.0000%	100.0000%
116	2412	99.0449%	98.5130%	99.5825%
117	1535	99.9024%	99.8049%	100.0000%
118	2275	99.9561 %	100.0000%	99.9123%
119	1987	99.0035%	100.0000%	98.0266%
121	1863	99.5185%	99.2000%	99.8390%
122	2476	99.9596%	99.9193%	100.0000%
123	1518	99.9011%	99.8024%	100.0000%
212	2748	100.0000%	100.0000 %	100.0000%
213	3251	99.6461%	99.6001 %	99.6921%
214	2262	98.3693%	98.2827%	98.4561%
215	3363	99.3929%	98.9095%	99,8810%
220	2048	100.0000 %	100.0000%	100.0000%
221	2427	96.7782%	96.0640%	97.5031%
234	2753	100.0000%	100.0000%	100.0000%

TABLE IV
RESULTS OF COMPARING THE AIPE ALGORITHM WITH OTHER METHODS FOR QRS DETECTION USING THE MIT-BIH ARRHYTHMIA DATABASE.

Method	F1	Se	+P
AIPE	99.4871%	99.3777%	99.5991%
Pan-Tompkins [8]	99.2539%	98.8516%	99.6682%
Chen *et al.* [50]	62.9018%	62.8888%	62.8929%
EMD [52]	71.6963%	65.4503%	99.6093%
Adaptive Threshold [51]	10.8868%	5.7624%	98.2885%
IPE	98.4778%	98.4925%	98.4681%

[2] A. J. Einstein, L. J. Shaw, C. Hirschfeld, M. C. Williams, T. C. Villines, N. Better, J. V. Vitola, R. Cerci, S. Dorbala, and P. Raggi, "International impact of covid-19 on the diagnosis of heart disease," *Journal of the American College of Cardiology*, vol. 77, no. 2, pp. 173–185, 2021.

[3] F. Morshedlou, N. Ravanshad, and H. Rezaee-Dehsorkh, "A low-power current-mode analog qrs-detection circuit for wearable ecg sensors," in *2018 25th National and 3rd International Iranian Conference on Biomedical Engineering (ICBME)*. IEEE, 2018, pp. 1–6.

[4] Q. Xue, Y. H. Hu, and W. J. Tompkins, "Neural-network-based adaptive matched filtering for qrs detection," *IEEE Transactions on biomedical Engineering*, vol. 39, no. 4, pp. 317–329, 1992.

[5] I. Saini, D. Singh, and A. Khosla, "Qrs detection using k-nearest neighbor algorithm (knn) and evaluation on standard ecg databases," *Journal of advanced research*, vol. 4, no. 4, pp. 331–344, 2013.

[6] Z. Zidelmal, A. Amirou, M. Adnane, and A. Belouchrani, "Qrs detection based on wavelet coefficients," *Computer methods and programs in biomedicine*, vol. 107, no. 3, pp. 490–496, 2012.

[7] S. Kadambe, R. Murray, and G. F. Boudreaux-Bartels, "Wavelet transform-based qrs complex detector," *IEEE Transactions on biomedical Engineering*, vol. 46, no. 7, pp. 838–848, 1999.

[8] J. Pan and W. J. Tompkins, "A real-time qrs detection algorithm," *IEEE transactions on biomedical engineering*, no. 3, pp. 230–236, 1985.

[9] V. X. Afonso, W. J. Tompkins, T. Q. Nguyen, and S. Luo, "Ecg beat detection using filter banks," *IEEE transactions on biomedical engineering*, vol. 46, no. 2, pp. 192–202, 1999.

[10] S. Sahoo, P. Biswal, T. Das, and S. Sabut, "De-noising of ecg signal and qrs detection using hilbert transform and adaptive thresholding," *Procedia Technology*, vol. 25, pp. 68–75, 2016.

[11] D. Yang and Y. Zhang, "A real-time qrs detector based on low-pass differentiator and hilbert transform," vol. 175, p. 02008, 2018.

[12] R. J. Oweis and B. O. Al-Tabbaa, "Qrs detection and heart rate variability analysis: A survey," *Biomedical science and engineering*, vol. 2, no. 1, pp. 13–34, 2014.

[13] A. Burguera, "Fast qrs detection and ecg compression based on signal structural analysis," *IEEE journal of biomedical and health informatics*, vol. 23, no. 1, pp. 123–131, 2018.

[14] G. M. Friesen, T. C. Jannett, M. A. Jadallah, S. L. Yates, S. R. Quint,

and H. T. Nagle, "A comparison of the noise sensitivity of nine qrs detection algorithms," *IEEE Transactions on biomedical engineering*, vol. 37, no. 1, pp. 85–98, 1990.

[15] S. Francesca, C. G. Carlo, L. Di Nunzio, F. Rocco, and R. Marco, "Comparison of low-complexity algorithms for real-time qrs detection using standard ecg database," *International Journal on Advanced Science, Engineering and Information Technology*, vol. 8, no. 2, p. 307, 2018.

[16] R. Gutiérrez-Rivas, J. J. Garcia, W. P. Marnane, and A. Hernández, "Novel real-time low-complexity qrs complex detector based on adaptive thresholding," *IEEE Sensors Journal*, vol. 15, no. 10, pp. 6036–6043, 2015.

[17] C. Q. Wu, Z. Wang, G. Chen, and D. Ferebee, "Recent advances and developments in mobile health," *Journal of healthcare engineering*, vol. 2018, 2018.

[18] M. Riedl, A. Müller, and N. Wessel, "Practical considerations of permutation entropy," *The European Physical Journal Special Topics*, vol. 222, no. 2, pp. 249–262, 2013.

[19] Z. Chen, Y. Li, H. Liang, and J. Yu, "Improved permutation entropy for measuring complexity of time series under noisy condition," *Complexity*, vol. 2019, 2019.

[20] H. Namazi and O. Krejcar, "Analysis of pregnancy development by complexity and information-based analysis of fetal phonocardiogram (pcg) signals," *Fluctuation and Noise Letters*, vol. 20, no. 04, p. 2150028, 2021.

[21] D. Bajić, V. ajić, and B. Milovanović, "Entropy analysis of covid-19 cardiovascular signals," *Entropy*, vol. 23, no. 1, p. 87, 2021.

[22] C. Bandt and B. Pompe, "Permutation entropy: a natural complexity measure for time series," *Physical review letters*, vol. 88, no. 17, p. 174102, 2002.

[23] J. S. Richman and J. R. Moorman, "Physiological time-series analysis using approximate entropy and sample entropy," *American Journal of Physiology-Heart and Circulatory Physiology*, 2000.

[24] B.-l. Hao, "Symbolic dynamics and characterization of complexity," *Physica D: Nonlinear Phenomena*, vol. 51, no. 1-3, pp. 161–176, 1991.

[25] A. Humeau-Heurtier, C.-W. Wu, and S.-D. Wu, "Refined composite multiscale permutation entropy to overcome multiscale permutation entropy length dependence," *IEEE signal processing letters*, vol. 22, no. 12, pp. 2364–2367, 2015.

[26] J. Lin, "Divergence measures based on the shannon entropy," *IEEE Transactions on Information theory*, vol. 37, no. 1, pp. 145–151, 1991.

[27] M. Costa, A. L. Goldberger, and C.-K. Peng, "Multiscale entropy analysis of complex physiologic time series," *Physical review letters*, vol. 89, no. 6, p. 068102, 2002.

[28] D. Cuesta-Frau, M. Varela-Entrecanales, A. Molina-Picó, and B. Vargas, "Patterns with equal values in permutation entropy: do they really matter for biosignal classification?" *Complexity*, vol. 2018, 2018.

[29] L. Zunino, F. Olivares, F. Scholkmann, and O. A. Rosso, "Permutation entropy based time series analysis: Equalities in the input signal can lead to false conclusions," *Physics Letters A*, vol. 381, no. 22, pp. 1883–1892, 2017.

[30] B. Fadlallah, B. Chen, A. Keil, and J. Principe, "Weighted-permutation entropy: A complexity measure for time series incorporating amplitude information," *Physical Review E*, vol. 87, no. 2, p. 022911, 2013.

[31] Y. Li, B. Geng, and S. Jiao, "Refined composite multi-scale reverse weighted permutation entropy and its applications in ship-radiated noise," *Entropy*, vol. 23, no. 4, p. 476, 2021.

[32] H. Azami and J. Escudero, "Amplitude-aware permutation entropy: Illustration in spike detection and signal segmentation," *Computer methods and programs in biomedicine*, vol. 128, pp. 40–51, 2016.

[33] Z. Li, Y. Cui, L. Li, R. Chen, L. Dong, and J. Du, "Hierarchical amplitude-aware permutation entropy-based fault feature extraction method for rolling bearings," *Entropy*, vol. 24, no. 3, p. 310, 2022.

[34] U. Parlitz, S. Berg, S. Luther, A. Schirdewan, J. Kurths, and N. Wessel, "Classifying cardiac biosignals using ordinal pattern statistics and symbolic dynamics," *Computers in biology and medicine*, vol. 42, no. 3, pp. 319–327, 2012.

[35] D. Xie, S. Hong, and C. Yao, "Optimized variational mode decomposition and permutation entropy with their application in feature extraction of ship-radiated noise," *Entropy*, vol. 23, no. 5, p. 503, 2021.

[36] K. Noman, D. Wang, Z. Peng, and Q. He, "Oscillation based permutation entropy calculation as a dynamic nonlinear feature for health monitoring of rolling element bearing," *Measurement*, vol. 172, p. 108891, 2021.

[37] L. Zunino, M. C. Soriano, and O. A. Rosso, "Distinguishing chaotic and stochastic dynamics from time series by using a multiscale symbolic approach," *Physical Review E*, vol. 86, no. 4, p. 046210, 2012.

[38] W. Aziz and M. Arif, "Multiscale permutation entropy of physiological time series," in *2005 Pakistan Section Multitopic Conference*. IEEE, 2005, pp. 1–6.

[39] C. Bian, C. Qin, Q. D. Ma, and Q. Shen, "Modified permutation-entropy analysis of heartbeat dynamics," *Physical Review E*, vol. 85, no. 2, p. 021906, 2012.

[40] J. A. Van Alste, W. Van Eck, and O. Herrmann, "Ecg baseline wander reduction using linear phase filters," *Computers and Biomedical Research*, vol. 19, no. 5, pp. 417–427, 1986.

[41] P. Ciarlini and P. Barone, "A recursive algorithm to compute the baseline drift in recorded biological signals," *Computers and biomedical research*, vol. 21, no. 3, pp. 221–226, 1988.

[42] C. Meyer and H. Keiser, "Electrocardiogram baseline noise estimation and removal using cubic splines and state-space computation techniques," *Computers and Biomedical Research*, vol. 10, no. 5, pp. 459–470, 1977.

[43] ——, "Electrocardiogram baseline noise estimation and removal using cubic splines and state-space computation techniques," *Computers and Biomedical Research*, vol. 10, no. 5, pp. 459–470, 1977.

[44] J. R. Gradwohl, E. W. Pottala, M. R. Horton, and J. J. Bailey, "Comparison of two methods for removing baseline wander in the ecg," in *Proceedings. Computers in Cardiology 1988*. IEEE, 1988, pp. 493–496.

[45] C. Meyer and H. Keiser, "Electrocardiogram baseline noise estimation and removal using cubic splines and state-space computation techniques," *Computers and Biomedical Research*, vol. 10, no. 5, pp. 459–470, 1977.

[46] S. Vieau and P. A. Iaizzo, "Basic ecg theory, 12-lead recordings, and their interpretation," in *Handbook of Cardiac Anatomy, Physiology, and Devices*. Springer, 2015, pp. 321–334.

[47] G. B. Moody, W. Muldrow, and R. G. Mark, "A noise stress test for arrhythmia detectors," *Computers in cardiology*, vol. 11, no. 3, pp. 381–384, 1984.

[48] G. B. Moody and R. G. Mark, "The impact of the mit-bih arrhythmia database," *IEEE Engineering in Medicine and Biology Magazine*, vol. 20, no. 3, pp. 45–50, 2001.

[49] S. Sarafan, T. Le, A. M. Naderi, Q.-D. Nguyen, B. T.-Y. Kuo, T. Ghirmai, H.-D. Han, M. P. Lau, and H. Cao, "Investigation of methods to extract fetal electrocardiogram from the mother's abdominal signal in practical scenarios," *Technologies*, vol. 8, no. 2, p. 33, 2020.

[50] H. Chen and S.-W. Chen, "A moving average based filtering system with its application to real-time qrs detection," in *Computers in Cardiology, 2003*. IEEE, 2003, pp. 585–588.

[51] I. I. Christov, "Real time electrocardiogram qrs detection using combined adaptive threshold," *Biomedical engineering online*, vol. 3, no. 1, pp. 1–9, 2004.

[52] S. Pal and M. Mitra, "Empirical mode decomposition based ecg enhancement and qrs detection," *Computers in biology and medicine*, vol. 42, no. 1, pp. 83–92, 2012.